The Distribution of Intracellular Ions in the Avian Salt Gland

S. BRIAN ANDREWS, JOSEPH E. MAZURKIEWICZ, and R. GARY KIRK
Department of Physiology, Yale University School of Medicine, New Haven, Connecticut 06510; and Department of Anatomy, Albany Medical College of Union University, Albany, New York 12208

ABSTRACT To investigate the mechanism of salt secretion in the avian salt gland, we used quantitative electron probe microanalysis to measure the intracellular elemental concentrations in dry cryosections of unspecialized and partially specialized secretory epithelial cells from fresh water- and salt water-adapted ducklings, respectively. In conjunction with this, human and duckling erythrocytes were also analyzed, since these provided the experimental basis for using in situ erythrocytes as standards for determining the local water content of epithelia from the analysis of dried cryosections.

The microprobe results from both types of erythrocytes compared favorably with chemical determinations of elemental concentrations. The nucleated avian erythrocytes, whose wet-weight elemental concentrations were determined by a compartmental analysis that required neither a peripheral standard nor a measure of the local mass, revealed a marked accumulation of P and K in the nucleus (388 and 190 mmol/kg wet wt, respectively) relative to the cytoplasm (67 and 85 mmol/kg wet wt). In both developmental states of the epithelial cells, the nucleus and apical cytoplasm had essentially similar and unremarkable concentrations of Na (76 and 83 mmol/kg dry wt, respectively, in the adapted cells vs. 72 and 81 mmol/kg dry wt in the control cells) and K (602 and 423 mmol/kg dry wt vs. 451 and 442 mmol/kg dry wt). Chloride, however, which was in general rather high, was significantly depressed in the apical cytoplasm of adapted cells only (164 and 124 mmol/kg dry wt in the nucleus and cytoplasm, respectively, of adapted cells ($P < 0.05$) vs. 138 and 157 mmol/kg dry wt for control cells ($P < 0.05$)). Cation concentrations (Na + K) were elevated ~15% in the basal regions of adapted cells as compared with apical cytoplasm.

When tissue water variations are accounted for, the results suggest that: *(a)* an active, energy-requiring process is responsible for chloride accumulation in this cell; *(b)* the apical membrane is a regulatory site for secretion; and *(c)* there are regional distinctions in the distribution of ions and water, particularly in the salt water-adapted cell. These conclusions are consistent with active chloride transport as the basis for salt secretion in this tissue.

A common mechanism, namely, active[1] chloride transport through the agency of a basolateral membrane-bound Na^+/Cl^- co-transport system (1), appears to account for net sodium chloride secretion in a number of exocrine tissues (2–6). The avian salt gland (7)—an epithelium which undergoes a dramatic morphological, developmental, and functional response to chronic osmotic stress (8)—may well invoke a similar mechanism to secrete a very hypertonic saline solution (9). In this case, as in the tissues cited above, this mode of transcellular ion movement might be reflected in the concentrations of intracellular electrolytes, particularly chloride. This appears to be the case in isolated dispersed duckling salt gland cells (10). However, the intact salt gland, because of its complex tubular anatomy at both the cell and tissue levels, is not particularly amenable to the chemical and electrophysiological approaches that so far have been used on chloride-transporting tissues. Therefore, we used quantitative, energy-dispersive x-ray microanalysis[2] to determine the intracellular elemental concentrations of the major electrolytes in the principal cells of duckling

[1] "Active transport" is used here to mean movement against an electrochemical gradient; no mechanistic implication is intended.

[2] The following are synonyms or acronyms for this mode of x-ray analysis: electron probe microanalysis (EPMA), electron microprobe analysis (EMA), and electron probe analysis (EPA).

THE JOURNAL OF CELL BIOLOGY · VOLUME 96 MAY 1983 1389-1399

salt gland in both control and salt water-adapted developmental states, and found positive evidence for active chloride transport in this tissue. Specifically, we find that (*a*) the intracellular concentration of chloride is almost certainly above electrochemical equilibrium, indicating chloride accumulation against an energy barrier and that (*b*) the cytosolic chloride concentration is reduced in secreting cells relative to control cells, implicating the apical membrane as the locus for the regulation of secretion.

As a prerequisite to the biological portion of this report, it is necessary to present certain methodological aspects of this study that were crucial to its feasibility. A particular example of such considerations was the need to reconcile the analysis of freeze-dried cryosections (required for the positive definition of cellular compartments in this complex tissue) with the fact that a biologically relevant interpretation of electrolyte concentrations required a knowledge of tissue water and possible variations in this parameter. Therefore, we also report the technical details that are essential for understanding and evaluating our implementation of quantitative, biological microanalysis. These results include the verification of this microprobe methodology using one- and two-compartment erythrocytes as model biological systems, and the derivation of two novel variations of existing approaches for estimating the original water content of freeze-dried tissue preparations. Preliminary accounts of portions of this study have been presented (11, 12).

MATERIALS AND METHODS

X-ray analysis was carried out on the following standard and experimental samples: (*a*) crystals of reagent-grade binary salts (13); (*b*) 20% (wt/wt) solutions of deionized bovine serum albumin (Sigma Chemical Co., St. Louis, MO) to which various amounts of electrolytes were added (14); (*c*) packed pellets of human erythrocytes in plasma prepared from whole blood that was collected in heparinized syringes from normal human volunteers; (*d*) similarly prepared packed pellets of duckling erythrocytes obtained from the whole blood of animals when killed; and (*e*) the salt glands of 15-d-old domestic ducklings, *Anas platyrhyncos,* that had been maintained on an *ad libitum* supply of duck mash and fresh water ("normal", "unstressed"), or that had been salt-adapted ("stressed") by drinking 1% saline only from day 9 until decapitation. Quantitative analysis was limited to the principal cells of the salt glands and specifically to those cells which were characterized as "unspecialized" in the fresh water-adapted duck and "partially-specialized" in the salt water-adapted bird (8). The morphological characterization of these developmental states, as well as the identification of these states in cryosectioned preparations, is discussed in Results.

Specimens for electron microscopy and x-ray analysis (except binary salts, which were prepared as described by Shuman et al. [13]) were prepared by quench-freezing followed by cryoultramicrotomy. In the case of protein solutions and erythrocyte suspensions, small drops on small copper pins or wooden dowels were quench-frozen essentially as described by Somlyo et al. (15) by plunging into rapidly stirred, supercooled Freon 22 (Virginia Chemicals, Portsmouth, VA) at −160°C; temperature was measured by a miniature (0.005 in.) copper/constantan thermocouple (Omega Engineering, Stamford, CT). Solid tissues such as salt gland were frozen similarly, after cutting into small pieces (<2 mm in the shortest dimension). The entire procedure from killing to freezing, and including excision and dissection, could be carried out in <15 s.

Chemical determinations of Na and K concentrations in protein solutions, plasma, and washed erythrocyte suspensions were obtained by flame photometry; dry mass fractions were determined gravimetrically. Prior to analysis, we washed erythrocytes to remove adherent plasma and extracellular ions (16). Specimens for conventional electron microscopy were prepared by immersion in 2.5% glutaraldehyde in 100 mM cacodylate buffer, pH 7.4, for 2 h, followed by postfixation for 1 h in 1% osmium tetroxide in the same buffer. After fixation, tissue blocks were washed, dehydrated through a graded series of ethanol solutions, and embedded in Epon 812. Thin sections were cut and stained with a saturated solution of uranyl acetate, followed by alkaline lead citrate, before viewing in a JEOL 100-CX electron microscope. Stereological techniques were used to estimate the volume fractions, V_v, of cell compartments in duckling erythrocytes (17). A square grid with 1-cm spacing was projected onto prints of electron micrographs at × 6,300 and evaluated by the "point-hit" method. Statistical evaluation of concentration differences was based on the two-tailed Student's *t* test for independent samples; $P < 0.05$ was the minimal criterion for significance.

Cryoultramicrotomy: We sectioned frozen biological samples using a Sorvall MT-2B microtome equipped with an FTS cryokit (Dupont Instruments, Inc., Newtown, CT) and modified to reduce the flow rate and turbulence of the cooling gas and to ameliorate the associated build-up of static charge. Sections were cut manually at very slow speeds using conventional glass knives (45° knife angle, 6° clearance angle) at temperatures of −105°C for epithelial tissue and −90°C for cell suspensions and protein solutions. Temperature was monitored by the previously described copper/constantan thermocouple placed directly on the shoulder of the specimen. The sections were obtained from the natural face of the frozen blocks, that is, the blocks were not trimmed. Sections for tissue analysis were ~130 nm thick after freeze-drying, while those for instrument calibration and testing ranged from <100 nm–1 μm. Specimen thickness could be inferred from the rate of continuum x-ray production and scanning transmission electron microscopy (STEM) contrast because the contrast response of the ETEC Autoscan electron microscope (Perkin-Elmer ETEC, Inc., Perkin-Elmer Corp., Hayward, CA) had been previously calibrated against interferometrically characterized standard films (18). With the aid of an eyelash brush, the sections were transferred from the back of the dry knife onto carbon foil-coated 100-mesh copper grids. Thereafter, the grids were sandwiched with a second coated grid, tacked with a chilled brass rod, freeze-dried at <−80°C and $<10^{-5}$ Torr (Denton DV-502 vacuum evaporator, Cherry Hill, NJ), separated and coated with a thin overcoat of carbon, essentially as described in detail by Somlyo et al (15).

Electron Probe Microanalysis: This section provides a detailed description of the methodology used for x-ray microanalysis because the methods used in this laboratory have not been described previously. This system and methodology are mainly evolved from the advances of others (13–15, 19). Energy-dispersive x-ray spectra were obtained using an ETEC Autoscan electron microscope equipped with a 30 mm^2 Kevex Si(Li) detector and a Kevex 7000 series x-ray spectrometer (Kevex Corp., Foster City, CA) interfaced to a PDP 11V03-L computer (Digital Equipment Corp, Maynard, MA). The flange for mounting the detector in the specimen chamber, as well as the STEM/x-ray specimen holder, were designed and fabricated from aluminum in this laboratory. The specimen holder included an integral Faraday cup and was painted with DAG 154 (Ted Pella, Inc., Tustin, CA). Certain later spectra were obtained on a newer instrument, a JEOL 100-CX. In this case, the instrument was equipped with a Kevex EDS detector in a configuration specified by the manufacturer, including a thick aperture above the objective lens ("hard x-ray aperture") and a machined carbon grid holder. Minor modification to this carbon insert and the bronze specimen rod permitted spectra to be acquired at a 35° tilt angle without significant absorption of soft x-rays. X-ray spectra were acquired at 10 eV/channel from specimens at ambient temperature using an accelerating voltage of 30 kV (ETEC) or 80 kV (JEOL), and a beam current of 1.0 nA for 100 s (livetime). Analyses performed on the same standard sections in both microscopes gave identical quantitative results, indicating that there was no systematic error introduced by differences in the two instruments; this might have occurred, for example, due to differences in stray background or accelerating voltage. Analyses were generally performed in STEM mode using small scanning rasters of <0.2–1.0 μm^2; the size and shape of the raster was fully adjustable and depended on the structure being analyzed. Under analytical conditions, the CRT images were comparable in quality to the micrographs shown in Figs. 5, 7, and 9. In addition, the STEM photomultiplier output was displayed in y-modulation mode on an auxilary X-Y monitor during analysis. Thus, the area chosen for analysis could be recognized by the contrast "grain" and any drift or contamination that might have occurred during analysis would have been immediately apparent.

Because the operating conditions for microanalysis were known to promote beam-induced specimen damage, we examined carefully the possibility of errors arising from mass loss and contamination artifacts. Using an approach similar to that of Dörge et al. (14), freeze-dried cryosections of electrolyte-doped albumin solutions were irradiated with electron doses that ranged from 6×10^{-3} - 1×10^{3} nC/μm^2; this six decade dose range was achieved by varying both the irradiating time and the size of the scanning raster at a constant beam current of 1 nA. The results are summarized in Fig. 1, where characteristic, continuum (2.89–3.19 keV) and total (0–10 keV) x-ray count rates are plotted as a function of time (and, therefore, also of dose). Both the total and continuum x-rays showed clear evidence of mass loss, as these x-ray intensities stabilized at ~75% of their initial rates after an applied dose of ~0.2 nC/μm^2; this critical dose did not depend on the beam current density, which itself varied over four orders of magnitude. Among the characteristic x-rays only the sulfur K line was radiation sensitive. The characteristic x-ray peaks of other elements of biological interest, and specifically including chloride, neither increased nor decreased as a function of time and dosage, up to doses as high as 10 nC/μm^2 and at beam current densities exceeding 10 nA/μm^2. Such doses did, however, produce contamination artifacts in some early experiments. In cases where the contamination artifact was <10%, a correction to the continuum was applied as previously described (12). Subsequent improvements in the operating environment of the microscopes made such corrections unnecessary in later experiments. To determine whether the conse-

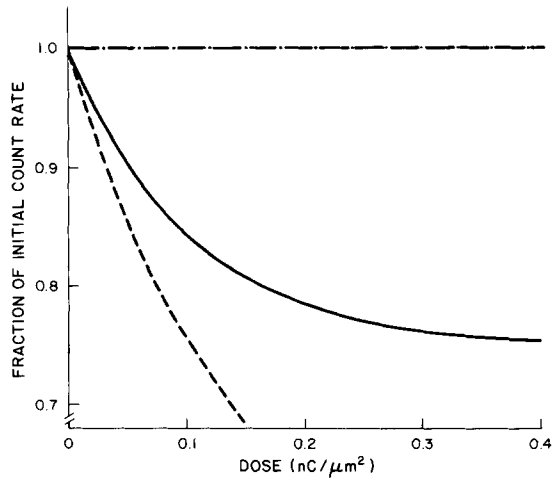

FIGURE 1 Dependence of x-ray count rates on electron dose. In the moderate dose regime, mass loss was evident from a decrease in count rate for total (0–10 keV) and continuum (2.89–3.19 keV) x-rays (—), as well as for the sulfur K emission (- - -). Potassium and chlorine K x-ray count rates (·-·-) were not sensitive to dose. These curves are composites of data from numerous sections of different quench-frozen solutions of electrolyte-doped 20% albumin.

quences of specimen/beam interactions as observed on albumin samples could be generalized to other biological materials, we examined sections of human and duckling erythrocytes, duckling salt gland, and rat and rabbit kidney parenchyma. The results regarding mass loss were essentially similar, although these could be interpreted only qualitatively since such specimens were compositionally heterogeneous at the level required for low dose measurements.

The quantitation approach used in this study was the multiple least-squares (ML) method developed for EDS data by Schamber (20). Our implementation of these calculations was essentially as described in detail by Shuman et al. (13), including the integration of characteristic peaks in experimental EDS spectra by convoluting the raw spectrum with a zero-weight digital filter to suppress background, followed by multiple least-squares fitting of the derivative spectrum. The tissue-derived continuum was then reconstructed by stripping the characteristic peaks and extraneous continuum contributions from the original spectrum. Corrections for grid-generated and other extraneous continuum components were scaled to the Cu L_α peak. However, the continuum was estimated in the 2.89–3.19 keV energy window, since the recommended range, centered at 1.5 keV (13), was precluded in one of our instruments by an Al K interference. In addition, the continuum was corrected for the support film contribution by subtracting the weighted average of the carbon film continuum in the vicinity of the section after determining that it was independent of the location within a grid square. In this case, the statistical variance was also recalculated.

The approaches used to derive elemental concentration and tissue mass fractions from characteristic and continuum x-ray intensities are based on the continuum normalization method (21, 22), which states that the elemental concentration per unit dry weight is proportional to the ratio of the characteristic x-ray intensity to the tissue-derived continuum intensity. This relationship is given in simplified form in Eq. 1:

$$C_x = W_x (I_x/B), \quad (1)$$

where C_x is the concentration of element x in mmols/kg dry wt., I_x is the integrated intensity of characteristic x-rays for this element, B is the continuum intensity arising from the specimen only within an arbitrary but constant energy window, and W_x is the configuration-dependent constant of proportionality. Although W_x is composed of fundamental parameters, it can most conveniently be determined empirically. Also, the calculation of I_x by ML fitting of digitally filtered spectra requires a file of reference spectra which contain characteristic peak energy and shape information for all elements that may occur in an experimental spectrum. Finally, the true tissue continuum, B, must be obtained by correcting the experimental continuum for extraneous contributions. Thus. calibration standards are required for all three terms on the right side of Eq. 1. Spectra for peak shape and position data were derived from either pure element standards or thick crystals of binary salts in which the component x-ray peaks were well separated, e.g., NaCl (cf. illustrative list in reference 13; also note that this approach introduces a small error in peak shape due to the effect of absorption edges for $Z < 14$). Thin crystals (<1 μm) of binary salts such as NaCl and KH_2PO_4 were also used to determine relatively the molar sensitivity coefficients of the two elements in a crystal, i.e., the ratio of W_x(cation)/W_x(anion). This procedure worked well, and afforded spectra of very good statistical quality, provided that certain precautions were observed. To eliminate absorption effects, the ratio of W_x(cation)/W_x(anion) should be determined by plotting this ratio vs. total x-ray counts (proportional to thickness) and evaluating the ratio at count rates in the range expected for tissue sections (Fig. 2). However, since the count rates from thin sections of tissue are very small, it is sufficient in practice to plot I_x(anion)/I_x(cation) (equal to W_x[cation]/W_x[anion]) vs. x-ray counts and extrapolate to zero counts. This precaution was most important with the low Z elements Na and Mg. Additionally, certain binary combinations which exhibit substantial secondary fluorescence effects must be treated similarly; KCl is the most obvious example (Fig. 2). A third type of standard, viz., freeze-dried cryosections of 20% albumin solutions containing known amounts of the elements Na, K, Cl, and/or P were also used (14). These specimens served to determine the absolute values of W_x when the continuum was generated by a protein matrix similar to that expected from freeze-dried constituents of cytoplasm. Furthermore, data from these albumin sections: (*a*) provided a cross-check on the relative value of W_x as derived from binary crystals; (*b*) allowed the calculation of absolute W_x values for elements not actually measured in albumin matrices; and (*c*) permitted the usual demonstration that, at least for these four elements, plots of peak/background ratio vs. known concentrations were linear (not shown). Fig. 3 illustrates the experimentally determined relationship between the coefficients W_x and the energy of the characteristic K_α x-ray lines.

The utility of Eq. 1 can be compromised by errors in the estimation of the continuum derived from the tissue only owing to mass loss effects. Therefore, corrections for this source of error were considered explicitly. With a beam current density of 1 nA/μm², full mass loss from protein matrices occurs in <1 s; thus, the x-ray data from intracellular compartments must reflect full mass loss conditions. Since the quantitation coefficients W_x were derived from albumin matrices which were known to suffer 25% mass loss under similar conditions, the W_x factors contain an implicit assumption of 25% mass loss. The quantitation scheme, therefore, will introduce a mass loss error only to the extent that this effect in cell compartments differs from 25%. Our present data, as well as many previous studies (e.g., references 14, 23), indicate that this should be a reasonably small error, since mass loss from cells and proteins consistently runs 15–25%.

The estimate of the tissue-derived continuum influences the analysis in a second way, since it is only through the continuum that one obtains a measure of the local water content of the tissue. The interpretation of the analytical results requires a knowledge of this parameter. In all experiments, primary data were obtained as concentrations per unit dry weight (mmol/kg dry wt), calculated from peak/continuum ratios as described (13). In this case, *relative* changes in water content were evaluated by analysis of continuum intensities from *paired* areas of tissue (25); the *absolute* water content associated with these analysis was inferred from independent measurements. In some instances, it was possible to obtain dry mass fractions and concentrations per unit wet wt (mmols/kg wet wt) directly by using variations of the internal standard ratios method (14); since these have not been detailed previously, they are fully described and compared with established methods below. (Note that the applicability of the internal

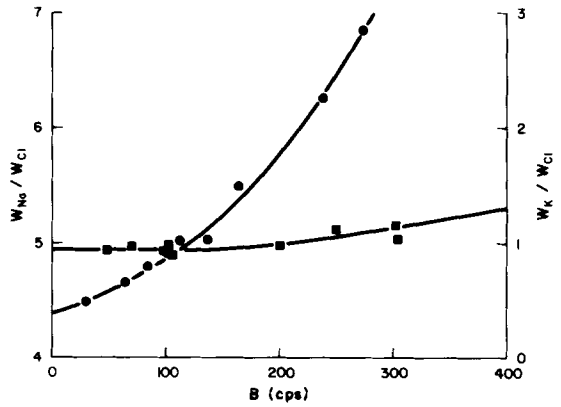

FIGURE 2 Effect of crystal thickness on W_x, the calibration constants that relate peak/continuum ratios to molar concentrations per unit dry weight. In this figure, the ratio of W(cation)/W(anion) for a binary salt is plotted against the specimen-only continuum radiation, B, which is itself proportional to crystal thickness. Left ordinate (●)—sodium chloride; the ratio rises rapidly with thickness due to increasing absorption of the soft Na K x-rays. Right ordinate (■)—potassium chloride; the ratio begins to rise above B = 100 cps due to an increase in the Cl signal at the expense of the K K line. Since the continuum count rate for tissue sections is typically <10 cps, W_x ratios can be approximately by extrapolating these curves to zero; in this case, W_{Na} has the largest uncertainty among the elements of biological interest.

standard method is still open to question because it requires assumptions regarding constancy of section thickness and beam current, regarding the microhomogeneity of peripheral standards, and regarding the absence of shrinkage artifacts during drying [22, 24].)

RESULTS

Methodological Verification

Since others have demonstrated that it is possible to prepare both thin (14) and ultrathin (15, 25) freeze-dried specimens that are suitably free from redistribution artifacts, we need only to demonstrate a satisfactory upper limit for such artifacts in the finished preparations of this study. Freeze-dried cryosections of 20% albumin solutions, such as illustrated in Fig. 4, demonstrated that the spaces due to ice damage averaged only 0.2 μm in diameter at a depth of 20 μm; this constitutes a worst-case estimate for the spatial dislocation of proteins and ions within intracellular compartments. Additionally, these sections had maintained an ice crystal size vs. depth profile (including the superficial layer of "vitreous" ice) (Fig. 4 *a*) that is consistent only with the initial freezing step; this implies the absence of any significant redistribution artifact resulting from recrystallization or melting that might have been introduced in steps following freezing. The size and pattern of ice crystal information within intracellular compartments in tissue sections were similar to the albumin standards (cf. Figs. 5, 7, and 9). Further, these preparations gave no morphological indications of gross differential shrinkage between compartments of different hydration which might impact quantitation by the internal standard approach (24).

Packed pellets of human erythrocytes were chosen as the first model tissue to examine by microanalysis, since these are simple, one-compartment cells with a well-known intracellular electrolyte composition. Excellent agreement was found between the results from x-ray and chemical analysis, as illustrated in Figs. 5 and 6, and summarized in Table I. Microanalysis was also carried out on the blood plasma, specifically to demonstrate the large and expected reversal of Na and K concentrations when the probe is localized outside the cells. This is evidence against the occurrence of sectioning artifacts such as "smearing" of a "melt zone." This conclusion is further supported by the observation that the quantitative results from sections of protein and erythrocyte standards at various thicknesses (<0.1–1 μm) were independent of thickness.

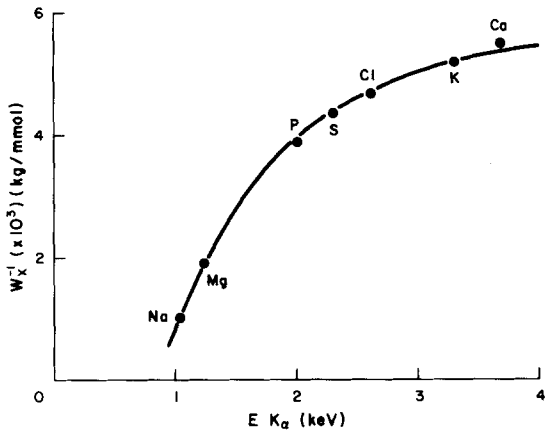

FIGURE 3 Change in W_x, the molar sensitivity constants, as a function of the energy of K x-ray emission. The points for low-Z elements of biological interest are identified. This curve is plotted as the reciprocal of W_x because in this form the height of the curve is directly proportional to K x-ray intensity of a given element at a constant concentration. As an example, the intensity of characteristic calcium K x-rays is 5.2 times greater than those of sodium at the same molar concentration.

Determination of Local Tissue Water from Dried Sections

An understanding of the cellular distribution of water is crucial to interpreting the microprobe data. If microanalysis is to be carried out on dry sections, however, then the contribution of tissue water must be determined indirectly. One well-documented approach, namely, obtaining concentrations per unit volume from peripheral standards (14), already exists for this purpose. Here we demonstrate the feasibility of two extensions of this strategy using two-compartment, nucleated erythrocytes of the domestic duckling—cells which are also of interest as a model for studying coupled ion transport (26, 27)—as a test system. The results provide: (*a*) an illustration of compartmental analysis as a means of determining wet weight concentrations from microanalysis of dried sections without recourse to internal standards; and (*b*) a characterization of the erythrocyte population in anticipation of its use as an internal standard for the analysis of intact epithelia. The following treatment extends a preliminary description of this approach (12), in that the equations are generalized to multicompartmental tissues, and more detail is provided in Table II and in the calculation of potassium concentrations.

For a multicompartmental tissue system in which all compartment have been recognized and analyzed in thin sections of uniform thickness, the absolute elemental concentration per unit volume (closely approximating wet-weight concentration) is uniquely specified by three factors: (*a*) the ratios of elemental concentrations between the various compartments; (*b*) the total concentration per volume of tissue; and (*c*) the volume-fraction of all compartments. The elemental ratios can be determined from the appropriate ratios of characteristic x-rays, and the latter two parameters can be measured by bulk chemical analysis and morphometry, respectively. The necessary relationships are given in Eqs. 2–4:

$$C_{x,T} = \sum_{i=1}^{n} V_{V,i}\, C_{x,i}, \tag{2}$$

$$I_{x,i}/C_{x,i} = I_{x,i+1}/C_{x,i+1} = \cdots = I_{x,n}/C_{x,n}, \tag{3}$$

$$\sum_{i=1}^{n} V_{V,i} = 1, \tag{4}$$

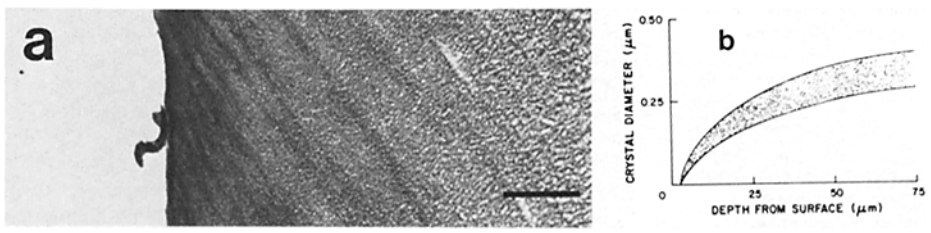

FIGURE 4 Dependence of ice crystal size and size distribution on distance from the sample surface. *(a)* Transmission electron micrograph of a freeze-dried cryosection of quench-frozen 20% albumin solution. Bar, 2 μm. × 5,400. *(b)* Graphical representation; the shaded area represents the range of void diameters measured at a given depth. Note the difference in scale between *a* and *b*.

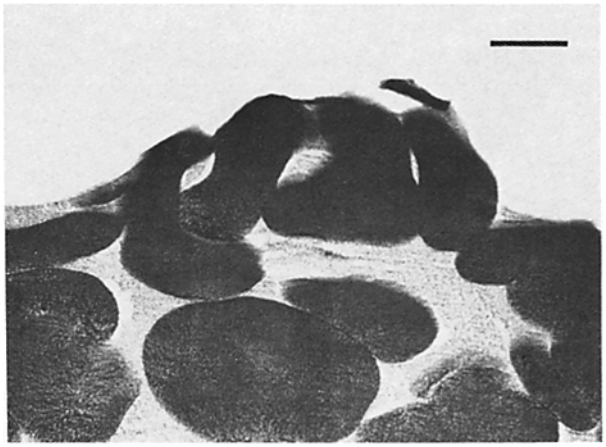

FIGURE 5 Transmission electron image of a freeze-dried cryosection of a packed pellet of human erythrocytes in plasma. The surface of the quench-frozen drop is at the top. The cells are relatively well-preserved, but the plasma matrix is not; a gradation of intracellular ice damage can be seen. Bar, 2 μm. × 5,400.

where C is the concentration in mmol/kg wet weight, V_V is the volume-fraction, I is the number of characteristic x-rays, x indicates a specific element (or the continuum), i is the index for tissue compartments, and T refers to the total concentration without regard to compartmental distribution. The practical application of these equations can be illustrated using the avian erythrocytes as two-compartment model systems, i.e., compartment 1 (i = 1) is the nucleus and compartment 2 (i = 2) is the cytoplasm. Figs. 7 and 8 show representative examples of cryosectioned preparations and EDS spectra, respectively, from which the results were obtained and Table II provides the data necessary for a specific calculation of intracellular potassium. The wet weight cytoplasmic potassium concentration given in column 6, Table II was calculated from the chemical analysis, the morphometric data, and the x-ray ratio $I_{K,1}/I_{K,2}$ (column 1, Table II) by inserting Eqs. 3 and 4 into Eq. 2,

$$C_{K,T} = V_{V,1}\,(I_{K,1}/I_{K,2})C_{K,2} + (1-V_{V,1})C_{K,2}, \quad (5)$$

rearranging,

$$C_{K,2} = C_{K,T}/(1 + V_{V,1}(I_{K,1}/I_{K,2} - 1), \quad (6)$$

substituting, and solving for $C_{K,2}$,

$$C_{K,2} = 100/(1 + 0.16\,[2.29 - 1]), \quad (7)$$
$$C_{K,2} = 83 \pm 2 \text{ mmol/kg wet wt.}$$

Subsequently, the nuclear K concentration was obtained from Eq. 3.

$$C_{K,1} = (I_{K,1}/I_{K,2})C_{K,2} = 2.29 \times 83, \quad (8)$$
$$C_{K,1} = 190 \pm 5 \text{ mmols/kg wet-wt.}$$

A similar approach was used to derive the compartmental dry mass fractions (Table II, column 7) from the ratio of corrected continuum counts (Table II, column 2). However, we emphasize that an estimate of the continuum is not explicitly required and neither is a peripheral standard.

Table II also illustrates two independent ways to derive *dry-weight* K concentrations. In the first case, the concentration $D_{K,i}$ (Table II, column 4) was determined from peak/continuum ratios, $I_{K,i}/B_i$ (Table II, column 1/column 2), using the Hall approach (Eq. 1). Alternatively, $D'_{K,i}$ (Table II, column 5)

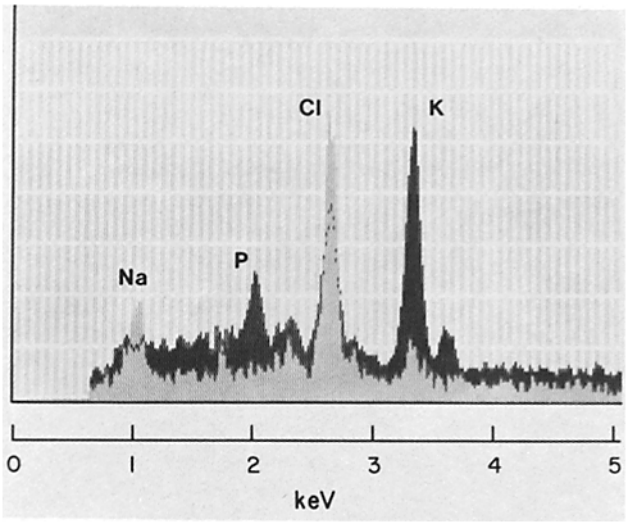

FIGURE 6 Energy-dispersive x-ray spectra from a representative paired analysis of a human erythrocyte (dark spectrum) and adjacent plasma (light spectrum); 100-s analysis time. Extraneous copper and silicon peaks have been subtracted by computer and a five-point smooth performed to enhance visual presentation.

TABLE I

Elemental Concentrations in Freeze-dried Sections of Erythrocytes

	Na	P	Cl	K	Dry weight fraction
		(mmol/kg wet weight)			*(g/100 g)*
Human erythrocytes					
Electron probe* (n = 28)	12 ± 2.0	20 ± 1.0	52 ± 1.8	84 ± 1.9	—
Chemical analysis	12‡	—	49	86‡	37
Human plasma					
Electron probe* (n = 9)	137 ± 12.1	0.4 ± 2.0§	105 ± 9.4	11 ± 3.6	—
Chemical analysis	146‡	—	105	5‡	6
Duckling erythrocytes					
Nucleus (n = 26)	5.5 ± 4.8§	388 ± 12.8	62 ± 2.5	190 ± 5.0	43 ± 1.9
Cytoplasm (n = 28)	2.0 ± 4.4§	67 ± 3.0	70 ± 2.7	85 ± 2.3	39 ± 1.7

Data are given as the mean ± SEM. The number of cells analyzed is indicated in parentheses.

* The wet weight concentrations were obtained by dividing the dry weight values from microanalysis by the dry mass fraction determined gravimetrically. In the case of plasma ions, relative concentrations were expressed as wet weight values by normalizing the characteristic x-ray intensities to the known plasma chloride concentration, 105 mmols/kg wet wt. None of the differences between chemical analysis and microanalysis are statistically significant (0.95 confidence level).

‡ Flame photometric determination paired with microprobe analysis.

§ Not significantly different from zero.

TABLE II

Compartmental Distribution of K in Normal Duckling Erythrocytes: Calculation of Wet- and Dry-weight Concentrations

	Relative x-ray counts*			K concentrations			
	$I_{K,i}$	B_i	$I_{K,i}/B_i$ ratio	$D_{K,i}$ dry wt.	$D'_{K,i}$ dry wt.	$C_{K,i}$ wet wt.	Dry wt.
Column Number	1	2	3	4	5 (mmol/kg)	6	7 (g/100 g)
Erythrocytes							
Microprobe Analysis							
Nucleus (i = 1)	1,000 ± 95	÷ 424 ± 67	→ 2.36 ± 0.40	→ 453 ± 76	= 442 ± 53	← 190 ± 19	÷ 43 ± 2.8
	÷	÷					
Cytoplasm (i = 2)	436 ± 61	÷ 384 ± 58	→ 1.14 ± 0.16	→ 216 ± 29	= 212 ± 25	← 83 ± 8.2	÷ 39 ± 2.6
	↓						
$I_{x,1}/I_{x,2}$ ratio	2.29 ± 0.39						
B_1/B_2 ratio		1.10 ± 0.24					
Whole cell					249	100	40
Chemical analysis					252	100 ± 8.0	40 ± 2.0
Literature values‡					231	92	40

Data are expressed as the weighted average ± SD of the paired analysis of nucleus/cytoplasm for 13 erythrocytes. Symbols in the heading are defined in the text. Arrows and arithmetic operators within the body of the table are intended to clarify the flow of the calculation. The morphometrically determined volume-fraction (V_v) of the nucleus for this sample of erythrocytes was found to be 0.16 ± 0.01 using electron micrographs of freeze-dried cryosections, and it was not significantly different if Epon sections from conventionally-embedded erythrocyte pellets were used.

* X-ray counts are normalized to $I_{K,1}$ = 1,000 in order to allow the inclusion and statistical comparison of data from sections with differing count rates due to, for example, variations in section thickness or beam current. These normalized values are given here to illustrate the various calculations of x-ray ratios, and to provide an indication of the statistics for the determination of characteristic x-rays. Because further calculations always utilize x-ray ratios, however, such normalization is superfluous and is not usually carried out. The actual range of count rates for $I_{K,1}$ was 52–100 cps.

‡ See reference 26.

FIGURE 7 Transmission electron micrograph of a freeze-dried cryosection of a packed pellet of duckling erythrocytes. Since the cells on the right were closer to the sample surface and were frozen with minimal ice crystal formation, the contrast difference between cell compartments is subtle and the nucleus is difficult to distinguish. Conversely, the deeper cells *(left)* were not as well preserved and the difference in degree of ice damage accentuates the cell compartments. Both types of cells had identical electrolyte compositions as determined by x-ray microanalysis. Bar, 1 μm. × 10,800.

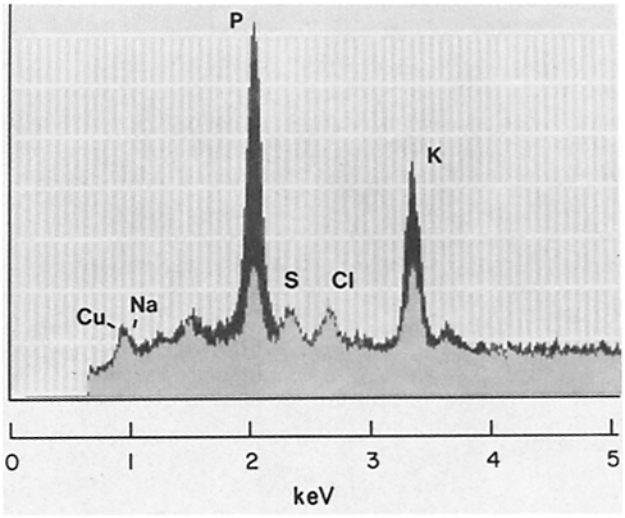

FIGURE 8 X-ray spectra of a duckling erythrocyte illustrating the differences between the nucleus (dark spectrum) and the cytoplasm (light spectrum). The localization of P and K in the nucleus is evident. Spectra have been stripped and smooth for presentation as described for Fig. 6.

was calculated as the wet weight concentration divided by the tissue dry mass fraction, i.e., column 6/column 7 (Table II). The results in Table II, columns 4 and 5, demonstrate good agreement between these two calculations of dry weight concentrations, and this will only occur if there is no significant absolute error in the determination of the tissue-derived continuum.

The strategy of complete compartmental analysis was used to determine the concentrations of the principal ions in duckling erythrocytes (Table I). The results revealed a decidedly asymmetrical distribution of elements; K and P were highly localized in the nucleus, while chlorine was slightly elevated in the cytoplasm and Fe was found exclusively in that compartment. Intracellular sodium levels, chemically determined as $C_{Na,T}$ = 4.8 mmol/L packed cells, were below the minimum detectable concentration for sodium in this system. The occurrence of such extreme concentration differences between nucleus and cytoplasm is an unusual finding by microanalysis. However, with the exception that we found no iron in the nucleus of these erythrocytes, these results are in good agreement with a previous quantitative microprobe study in which frozen-hydrated sections of developing chick embryo erythrocytes were analyzed (28). Thus, these findings may be a general feature of nucleated erythrocytes and may reflect a distinctive nuclear organization of these cells.

Duckling Salt Gland

The morphology of freeze-dried cryosections of salt gland epithelial cells is illustrated in Fig. 9 in comparison to conventional plastic sections. The cryosections compared favorably with respect to the preservation and recognition of characteristic morphology of this tissue, e.g., the complex interdigitations of lateral cell processes, the distribution of the abundant mitochondria and the cell-cell relationships which define the tubule lumen and overall tubule organization. It was also possible to identify with some certainty the developmental stages of various tubules based on established morphological criteria (cf. references 8 and 29 for a discussion of these criteria and references 8, 29, 30, 31 for examples of the various developmental stages as seen by electron microscopy). The principal cells of these tubules were analyzed in two distinct states: (*a*) unspecialized cells from fresh water-adapted animals, which were characterized by flat basal membranes and only moderate lateral interdigitations (Fig. 9 *a* and *b*); and (*b*) partially specialized cells from salt-adapted ducklings, which were recognized by the moderate convolution of the basal membrane and more extensive lateral infoldings (Fig. 9 *c* and *d*). The latter state was chosen because, despite the small size and elaborate morphology of the cells, moderately sized analytical probes ($<0.2\ \mu m^2$) could be accurately placed on identifiable subcellular areas. The analysis of the very complex, fully specialized cells would have entailed considerable uncertainty in probe localization. Measurements were obtained from three subcel-

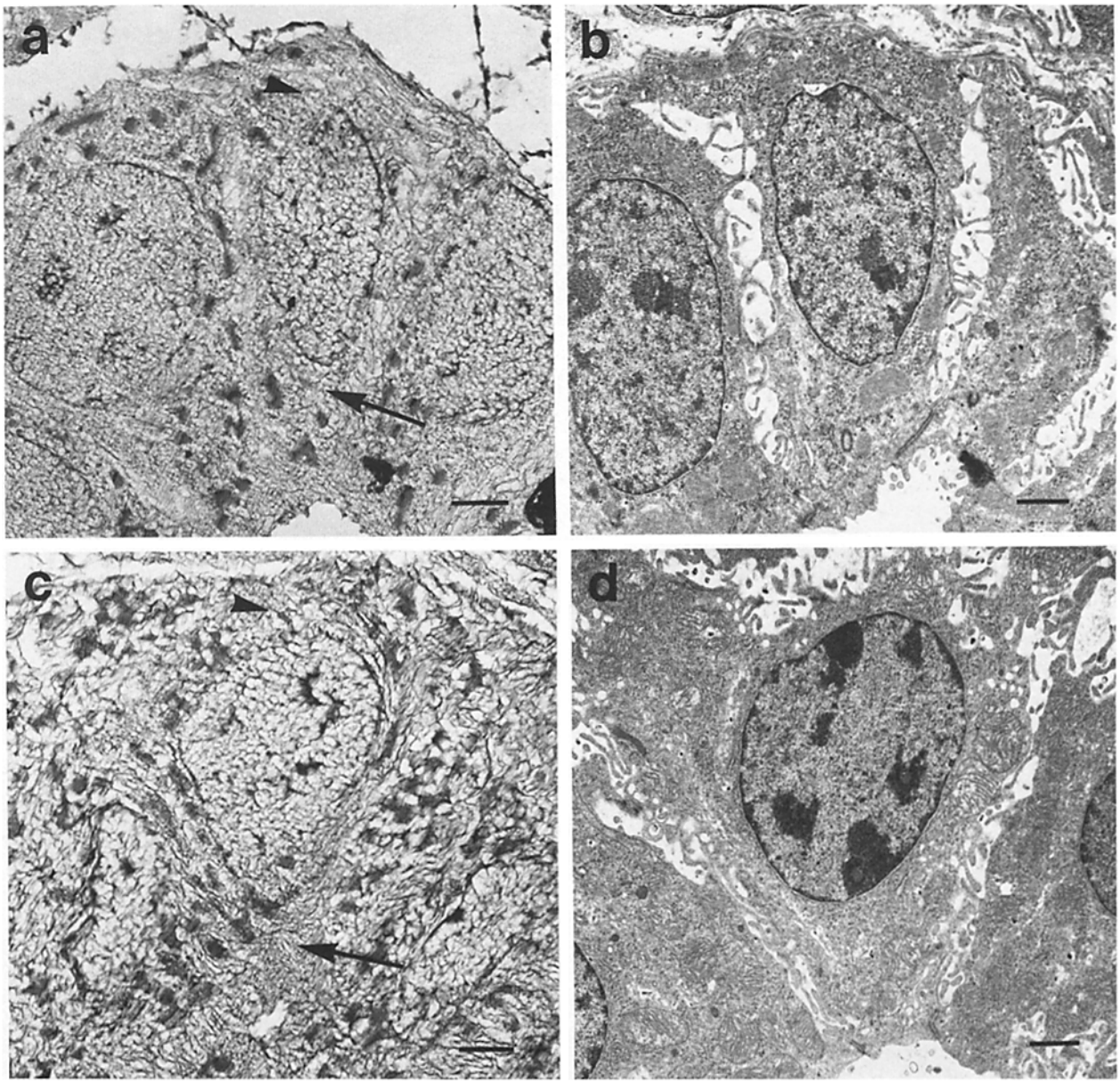

FIGURE 9 Transmission electron micrographs of principal cells of duckling salt gland tubules. *a* and *b* illustrate the similarity between an unfixed, unstained freeze-dried cryosection *(a)* and a conventional thin section of an Epon-embedded preparation *(b)*. Both micrographs demonstrate morphologically unspecialized principal cells from fresh water-adapted ducklings, as evidenced by the relatively simple cuboidal cell shape and the flat basal membrane with only moderate lateral interdigitations and a normal complement of mitochondria. *c* and *d* illustrate the same comparison for partially specialized secretory cells from salt water-adapted ducklings. These cells have a more complex shape, with significant amplification of the basal membrane, more extensive lateral infoldings, and abundant mitochondria. The arrows on *a* and *c* indicate typical areas for microanalysis of Region A, "apical cytoplasm," while the arrowheads identify Region B, "basal cytoplasm." Bars, 1 μm. (*a*) × 8,200; (*b* and *c*) × 8,000; (*d*) × 7,800.

TABLE III

Distribution of Elemental Dry Weight Concentrations in Duckling Salt Gland

	Na	P	Cl	K	Continuum
		(mmol/kg dry wt)			*(counts)*
Salt gland epithelial cells					
Salt water adapted					
Region A, cell apex (n = 12)	83 ± 18*	572 ± 22	124 ± 11‡	423 ± 14*‡	1,021 ± 27*‡
Region N, nucleus (n = 19)	76 ± 23	668 ± 37	164 ± 13‡	602 ± 22	798 ± 24*
Region B, cell base (n = 17)	125 ± 11*	596 ± 20	155 ± 8	469 ± 12*‡	1,134 ± 23*‡
Fresh water adapted					
Region A, cell apex (n = 9)	81 ± 11	525 ± 24	157 ± 7‡	442 ± 22	1,133 ± 57
Region N, nucleus (n = 17)	72 ± 17	629 ± 30	138 ± 4‡	451 ± 9	1,123 ± 28
Region B, cell base (n = 8)	140 ± 19	519 ± 5	183 ± 10	459 ± 31	1,079 ± 24

Data are given as the mean ± SEM. The number of cells analyzed is indicated in parentheses. The definition of subcellular regions is discussed in the text and illustrated in Fig. 9. Symbols are defined in the text.

* Significantly different, $P < 0.01$: $(D_{Na} + D_K)_{apex} - (D_{Na} + D_K)_{base}$ in salt-adapted cells; $B_{apex} - B_{nuc}$ and $B_{base} - B_{nuc}$ in adapted cells.

‡ Significantly different, $P < 0.05$: $(D_{Cl})_{apex} - (D_{Cl})_{nuc}$ in both salt-adapted and nonadapted cells; $(D_K)_{apex} - (D_K)_{base}$ in adapted cells; $B_{apex} - B_{base}$ in adapted cells.

TABLE IV

Distribution of Elemental Wet Weight Concentrations in Duckling Salt Gland

	Na	P	Cl	K	Continuum
		(mmol/kg wet weight)			*(g/100 g)*
Salt gland epithelial cells					
Salt water adapted*					
Region A, cell apex (n = 12)	23 ± 5.2	153 ± 5.8	33 ± 2.9	110 ± 3.8	24.6 ± 0.8
Region N, nucleus (n = 19)	12 ± 3.7	120 ± 7.2	33 ± 2.5	116 ± 4.2	19.2 ± 0.9
Region B, cell base (n = 17)	34 ± 3.1	160 ± 5.5	43 ± 2.2	128 ± 3.4	27.3 ± 0.9
Fresh water adapted‡					
Region A, cell apex (n = 9)	20 ± 2.7	131 ± 8.0	39 ± 2.3	111 ± 7.1	25§
Region N, nucleus (n = 17)	18 ± 4.1	158 ± 8.1	34 ± 1.2	113 ± 3.2	25§
Region B, cell base (n = 8)	35 ± 4.8	130 ± 3.3	46 ± 2.7	115 ± 8.4	25§

Data are given as the mean ± SEM. The number of cells analyzed is indicated in parentheses. The definition of subcellular regions is discussed in the text and illustrated in Fig. 9. Symbols are defined in the text.

* These concentrations are independent primary data, obtained using in situ erythrocytes as internal standards. The relevant values for the standard erythrocytes were: $I_{K,nuc}$ = 3,693 counts, $C_{K,nuc}$ = 171 mmols/kg wet wt; $I_{K,cyt}$ = 1,789 counts, $C_{K,cyt}$ = 83 mmols/kg wet wt; B_{nuc} = 1,533 counts, dry mass = 36.9 g/100 g; and B_{cyt} = 1,440 counts, dry mass = 34.7 g/100 g.

‡ Derivative results, obtained by multiplying the dry weight concentrations from Table III by an assumed dry mass fraction of 25 g/100 g; the SEM's were propagated using the experimental variances of the continua. This data is presented solely for the convenience of comparing fresh and salt water-adapted ducklings in similar units.

§ Value assumed for consistency with literature (32).

lular regions: region A (Fig. 9, arrows), the apical region where the probe could be unequivocally located on the cytoplasm[3] of a single cell; Region N, the nucleus; and Region B (Fig. 9, arrowheads), the basal region which was anticipated to reflect primarily cytosol, but very likely includes contributions from mitochondria, intercellular spaces, and neighboring cells. The results of this analysis are given in Table III in mmol/kg dry wt. However, as previously discussed, it is also desirable to express the elemental concentrations in units which take account of the local tissue water. To achieve this in the case of the salt-stressed gland, we adopted a variation of the internal standard proportionation method. Since the stressed gland is highly vascularized, a given section of this tissue frequently contained several well-preserved erythrocytes within the intertubular microvessels. These cells, whose elemental concentrations and water content were well known from prior chemical and electron probe analysis of the blood of the same duckling, could therefore be analyzed in situ in conjunction with the epithelial cells, and subsequently be employed as physiological internal standards. The wet weight concentrations for stressed salt gland principal cells given in Table IV were calculated using this approach. Unfortunately, this method was not applicable to the control glands, since this tissue is poorly perfused and suitable erythrocytes were encountered only rarely. Therefore, dry-weight concentrations were converted to wet-weight results (Table IV) in this case by assuming a cellular water content of 75 g/100 g. This value was chosen because it is generally consistent with the water content of transporting epithelial cells, and especially that of fresh water-adapted seagull salt gland (32). The assumption of uniform mass distribution follows from a statistical analysis of the x-ray continua (Table III) that implied no significant mass differences between subcellular regions. We emphasize that this calculation is solely for the convenience of comparing normal and salt-adapted epithelia in alternative and physiologically interesting units; the absolute value of the dry mass does not materially affect any of the conclusions drawn from these data, since all statistical comparisons are based on dry weight concentrations.

The results in Tables III and IV include three general observations that are in good agreement with other quantitative microprobe studies of epithelia (e.g., references 24 and 33). In contrast to the nucleated erythrocytes, a comparison of Region A with Region N in epithelial cells, taking account of local water variations, did not indicate a significant compartmentalization of cations between the nucleus and the cytoplasm.

[3] In this context, "cytoplasm" does not exclude the presence of small membrane-bound organelles, e.g., endoplasmic reticulum, which would not be recognized because of the level of ice damage in these preparations.

Furthermore, the intracellular concentrations of Na and K were well within the range expected for a prototypical epithelial cell. These concentrations did, however, differ significantly from chemical measurements of intracellular concentrations on a variety of intact avian salt glands (32, 34, 35), the microprobe data indicating lower cell Na and higher K. This has been a recurring observation when comparing x-ray microanalysis and bulk chemical analysis; Rick and co-workers (33, 36, 37) have argued that the discrepancy reflects the difficulties in extracellular space estimation that are inherent in the bulk analysis. In support of this view, we note that the present microprobe results are in very good agreement with the recent chemical determination (10) of intracellular electrolytes in *dispersed* salt gland cells.

With regard to results that bear on the secretory function of this tissue, three observations appear pertinent. Firstly, the chloride concentration is relatively high, i.e., >120 mmol/kg dry wt (>30 mmol/kg wet wt), in all cellular compartments. Secondly, the apical cytosolic chloride concentration does not appear to be higher than the corresponding nuclear concentration on either a dry weight or wet weight basis in the salt-adapted cells (124 vs. 164 mmol/kg dry wt, respectively, $P < 0.05$; 33 vs. 33 mmol/kg wet wt, difference not significant). This is in contrast to the control salt gland cells (157 vs. 138 mmol/kg dry wt, respectively, $P < 0.05$), and to a variety of other cell types (e.g., 24, 25, 33), in which the cytoplasmic chloride concentration is invariably higher than the nuclear chloride. Lastly, Region B, the region dominated by basal cytoplasm, appears to have elevated Na and/or K levels, at least in the stressed state (~30 and 130 mmol/kg wet wt, respectively; $P < 0.01$ for a comparison of apical [Na + K] with basal [Na + K] and $P < 0.05$ for apical K vs. basal K in stressed cells).

DISCUSSION

We have described a quantitative energy-dispersive x-ray microanalysis system, and have offered evidence using model and experimental biological systems that this instrument is capable of providing accurate and reliable data on intracellular ion concentrations. Further, the results show that this technique can be applied to a morphologically complex cell type and that results which recognize the role of cell water can be derived from data on dry sections. Since these findings confirm that microanalysis is suitable for such tissues, we have applied this technique to a study of electrolyte secretion in the avian salt gland.

It is now appreciated that in a variety of tissues, sodium chloride secretion occurs by active, transcellular transport of chloride (1). The generally accepted mechanism uses the inwardly directed sodium gradient to drive the accumulation of chloride through a neutral, Na-coupled cotransport carrier located in the basolateral membrane; subsequently, chloride is passively translocated across the apical membrane by electrical forces. Ultimately, the energy for transport derives from the maintenance of the sodium gradient by the basolateral Na^+-K^+-ATPase. It has been recognized that this process is characterized by the coupling of secretion to Na^+-K^+-ATPase activity, by the Na- and Cl-dependence of the uptake step, and by the sensitivity of this step to diuretic agents such as furosemide. Recent evidence has suggested that in some tissues the operation of this mechanism is reflected at the subcellular level by the accumulation of intracellular chloride in excess of electrochemical equilibrium (2, 38, 39) and by a secretagogue-induced change in apical membrane chloride permeability (39–43). With respect to the avian salt gland, the dependence of secretion on Na^+-K^+-ATPase activity was implied some time ago by studies of osmotic stress in intact animals (44); in view of the basolateral localization of the sodium pump, it was later proposed that this tissue might also employ an active chloride transport mechanism (9). Recent studies on isolated, dispersed cells (10) offer additional evidence to support this proposal. The present study, using an entirely independent approach, provides results in good agreement with those from isolated cells, and suggests, albeit indirectly, that two proposed characteristics of active chloride secretion, viz., energy-requiring chloride accumulation and reduced apical membrane chloride permeability in secreting cells, occur in intact salt gland.

These conclusions arise from the following considerations. The x-ray microanalysis results indicate that the cytoplasmic chloride concentration, as estimated using the data from the apical cell compartment, is 157 mmol/kg dry wt in the unstressed gland. This value for intracellular chloride implies active accumulation, since it is almost certainly greater than the concentration required for electrochemical equilibrium. This conclusion is justified even though we do not have certain information which is necessary to properly calculate the driving forces. Using reasonable and/or conservative assumptions regarding these unknown parameters (namely, that the dry mass of the cell is 25 g/100 g, that the basolateral membrane potential is −50 mV, that the chloride concentration in the lamina propria is 150 mM, that activity coefficients are equal in all compartments, and that electrolytes are totally dissolved in tissue water), it can be estimated that the equilibrium intracellular chloride concentration is <65 mmol/kg dry wt. This is 40% of the actual concentration. The difference is large enough that no plausible values for the estimated parameters would alter the interpertation. The second result that bears on the idea of active chloride transport is the relatively low cytosolic chloride concentration in the salt-adapted cells. Similarly low values have been obtained in other chloride-secreting tissues, either by chemical or activity measurements, and been explained by postulating that the chloride permeability of the apical membrane is higher in the secreting cells (42). Such an explanation would be fully consistent with the present results, but this point requires further clarification. Although it is now generally agreed that a change in membrane chloride permeability accompanies secretory stimulation, a change in intracellular chloride concentration does not necessarily follow from this, and such a change is not always seen. For example, a recent microanalysis study reported no change in chloride concentration in frog cornea cells upon stimulation with isoproterenol, although intracellular Na increased ~20% under these conditions (45).

Our results offer no insight into the involvement of Na in the salt gland transport process, because (*a*) no significant differences or changes were found in intracellular sodium concentrations in apical and nuclear compartments (although this is still consistent with a sodium requirement for chloride uptake), (*b*) the precision of sodium quantitation in these experiments was relatively low owing primarily to tubule-to-tubule variations, and (*c*) positive changes in tissue sodium which were observed in the basal region of these cells (Region B) are difficult to interpret for reasons discussed below. Regarding the differences between this and other studies, it is noted that the salt gland could be mechanistically distinct from other tissue models for chloride secretion, since in the salt gland the acute secretory response is elicited by cholinergic

stimulation, possibly mediated by cGMP (46), rather than by a cAMP-mediated process. Furthermore, this study has compared the functionally competent cell with its nonadapted, nonfunctional counterpart; that is, there is a developmental difference between the experimental and control states. Most other studies have used competent but nonstimulated cells as the control condition.

Another area of interest concerns the elemental concentrations found for the basal "cytoplasm" (Region B); most notably in the salt-adapted state, these are different from concentrations in the apical cytoplasm, and therefore imply compositional differences between regions of a cell not separated by membrane barriers. Moreover, certain trivial explanations are not wholly satisfactory. Thus, these data do not appear to be the result of a technical artifact, such as redistribution due to freezing damage or melting during cryoultramicrotomy; none of these occurrences is consistent with the maintenance of typically intracellular K, P, and dry mass levels in the basal region. A similar viewpoint can be used to assess extracellular contributions to the data; these were probably unavoidable in view of the complexity of the membrane infoldings in this region and the modest resolution of these analyses. In the case of the nonadapted cells, a contribution of ~10% of typical extracellular fluid (160 mM Na, 125 mM Cl, 6 g/100 g dry mass) would account for the elevated levels of Na and Cl (relative to the apical cytoplasm), and anticipated reductions in P, K, and dry mass would be small and within experimental error. For the stressed cells, however, a 10% extracellular space contribution, while it would adequately explain elevated Na and Cl concentrations, would only accentuate already significant differences between apical and basal potassium concentrations and dry mass. Thus, we conclude that cation concentrations (either K or Na + K) and dry mass fractions may be elevated in the basal region of salt-adapted cells. A similar possibility has been raised with respect to the basal regions of rat renal tubules (33). It is, of course, possible that the intercellular spaces do not have a composition similar to plasma. For example, this fluid could be low in Cl (24) or high in K (19, 47). While such considerations might change the identity and intra-/extracellular distribution of excess ions, they would not alter the conclusion that this excess exists. Since it is unlikely that these concentration differences between apex and base reflect a chemical potential difference of corresponding magnitude, it appears that some fraction of the ions in the basal region of this cell must contribute less, or not at all, to solute chemical activity. We speculate that this could occur as a consequence of differential binding or compartmentalization of solutes in the basal regions of this cell, or due to a regional change in the activity coefficient following from differences in the amount, identity, and/or distribution of the major cell proteins.

The authors are grateful to Drs. H. Shuman, A. P. Somlyo, and A. V. Somlyo for sharing with us their algorithm for the multiple least-squares fitting of EDS spectra.

This work was supported in part by National Institutes of Health grants HL-25775, AM-21391, GM-27574, and AM-17433, and by National Science Foundation grant PCM-7725208.

Received for publication 30 October 1981, and in revised form 15 November 1982.

REFERENCES

1. Frizzell, R. A., M. Field, and S. G. Schultz. 1979. Sodium-coupled chloride transport by epithelial tissues. *Am. J. Physiol.* 236:F1–F8.
2. Silva, P., J. Stoff, M. Field, L. Fine, J. N. Forrest, and F. H. Epstein. 1977. Mechanism of active chloride secretion by shark rectal gland: role of Na-K-ATPase in chloride transport. *Am. J. Physiol.* 233:F298–F306.
3. Zadunaisky, J. A. 1966. Active transport of chloride in frog cornea. *Am. J. Physiol.* 211:506–512.
4. Olver, R. E., B. Davis, M. G. Marin, and J. A. Nadel. 1975. Active transport of Na^+ and Cl^- across the canine tracheal epithelium in vitro. *Am. Rev. Respir. Dis.* 112:811–815.
5. Karnaky, K. J., Jr., K. J. Degnan, and J. A. Zadunaisky. 1977. Chloride transport across isolated opercular epithelium of Killifish: a membrane rich in chloride cells. *Science (Wash. DC).* 195:203–205.
6. Frizzell, R. A., M. J. Koch, and S. G. Schultz. 1976. Ion transport by rabbit colon. I. Active and passive components. *J. Membr. Biol.* 37:297–316.
7. Peaker, M., and J. L. Linzell. 1975. Salt Glands in Birds and Reptiles. Cambridge University Press, Cambridge.
8. Ernst, S. A., and R. A. Ellis. 1969. The development of surface specialization in the secretory epithelium of the avian salt gland in response to osmotic stress. *J. Cell Biol.* 40:305–321.
9. Ernst, S. A., and J. W. Mills. 1977. Basolateral plasma membrane localization of ouabain-sensitive sodium transport sites in the secretory epithelium of the avian salt gland. *J. Cell Biol.* 75:74–94.
10. Hootman, S. R., and S. A. Ernst. 1981. Effect of methacholine on Na^+ pump activity and ion content of dispersed avian salt gland cells. *Am. J. Physiol.* 241:R77–R86.
11. Andrews, S. B., J. E. Mazurkiewicz, and R. G. Kirk. 1980. Electron probe microanalysis of transporting tissues: duckling erythrocytes and salt-secreting epithelium. *In* Microbeam Analysis—1980. D. B. Wittry, editor. San Francisco Press, San Francisco. 255–258.
12. Andrews, S. B., J. E. Mazurkiewicz, and R. G. Kirk. 1981. Electron microprobe analysis of secretory epithelia: avian salt gland. *In* Microprobe Analysis of Biological Systems. T. E. Hutchinson and A. P. Somlyo, editors. Academic Press, New York. 21–46.
13. Shuman, H., A. V. Somlyo, and A. P. Somlyo. 1976. Quantitative electron probe microanalysis of biological thin sections: method and validity. *Ultramicroscopy.* 1:317–339.
14. Dörge, A., R. Rick, K. Gehring, and K. Thurau. 1978. Preparation of freeze-dried cryosections for quantitative x-ray microanalysis of electrolytes in biological soft tissues. *Pflügers Arch. Eur. J. Physiol.* 373:85–97.
15. Somlyo, A. V., H. Shuman, and A. P. Somlyo. 1977. Elemental distribution in striated muscle and the effects of hypertonicity. Electron probe analysis of cryosections. *J. Cell Biol.* 74:828–857.
16. Sachs, J. R. 1971. Ouabain-sensitive sodium movements in the human red blood cell. *J. Gen. Physiol.* 57:259–282.
17. Weibel, E. R., and R. P. Bollender. 1973. Stereological techniques for electron microscopic morphometry. *In* Principles and Techniques of Electron Microscopy: Biological Applications. M. A. Hayat, editor. Van Nostrand Reinhold, New York. 3:237–296.
18. Halloran, B. P., R. G. Kirk, and A. R. Spurr. 1978. Quantitative electron probe microanalysis of biological thin sections: the use of STEM for measurement of local mass thickness. *Ultramicroscopy.* 3:175–184.
19. Gupta, B. L., T. A. Hall, and R. B. Moreton. 1977. Electron probe x-ray microanalysis. *In* Transport of Ions and Water in Animals. B. L. Gupta, R. B. Moreton, J. L. Oschman, and B. J. Wall, editors. Academic Press, London, 83–143.
20. Schamber, F. H. 1977. A modification of the linear least-squares fitting method which provides continuum suppression. *In* X-ray Fluorescence Analysis of Environmental Samples. T. G. Dzubay, editor. Ann Arbor Science Publishers, Ann Arbor, MI. 241–257.
21. Hall, T. A. 1971. The microprobe assay of chemical elements. *In* Physical Techniques in Biological Research. G. Oster, editor. 2nd edition. Academic Press, New York. 1A:157–275.
22. Hall, T. A. 1979. Problems of the continuum-normalization method for the quantitative analysis of sections of soft tissue. *In* Microbeam Analysis in Biology. C. P. Lechene and R. R. Warner, editors. Academic Press, New York. 185–208.
23. Stenn, K., and G. F. Bahr. 1970. Specimen damage caused by the beam of the transmission electron microscope, a correlative reconsideration. *J. Ultrastruct. Res.* 31:526–550.
24. Gupta, B. L. 1979. The electron microprobe x-ray analysis of frozen-hydrated sections with new information on fluid transporting epithelia. *In* Microbeam Analysis in Biology. C. P. Lechene and R. R. Warner, editors. Academic Press, New York. 375–408.
25. Somlyo, A. P., A. V. Somlyo, and H. Shuman. 1979. Electron probe analysis of vascular smooth muscle: composition of mitochondria, nuclei, and cytoplasm. *J. Cell Biol.* 81:316–335.
26. Schmidt, W. F., III, and T. J. McManus. 1977. Ouabain-insensitive salt and water movements in duck red cells. I. Kinetics of cation transport under hypertonic conditions. *J. Gen. Physiol.* 70:59–79.
27. Palfrey, H. C., and P. Greengard. 1981. Hormone-sensitive ion transport systems in erythrocytes as models for epithelial ion pathways. *Ann. NY Acad. Sci.* 372:291–308.
28. Jones, R. T., R. T. Johnson, B. L. Gupta, and T. A. Hall. 1979. The quantitative measurement of electrolyte elements in nuclei of maturing erythrocytes of chick embryo using electron-probe x-ray microanalysis. *J. Cell Sci.* 35:67–85.
29. Martin, B. J., and C. W. Philpott. 1973. The adaptive response of the salt glands of adult mallard ducks to a salt water regime: an ultrastructural and tracer study. *J. Exp. Zool.* 186:111–122.
30. Hossler, F. E., M. P. Sarras, Jr., and E. R. Allen. 1978. Ultrastructural, cyto- and biochemical observations during turnover of plasma membrane in duck salt gland. *Cell Tissue Res.* 188:299–315.
31. Hootman, S. R., and S. A. Ernst. 1980. Dissociation of avian salt gland: separation procedures and characterization of dissociated cells. *Am. J. Physiol.* 238:C184–C195.
32. Schmidt-Nielsen, B. 1976. Intracellular concentrations of the salt gland of the herring gull *Larus argentatus. Am. J. Physiol.* 230:514–521.
33. Beck, F., R. Bauer, U. Bauer, J. Mason, A. Dörge, R. Rick, and K. Thurau. 1980. Electron microprobe analysis of intracellular elements in the rat kidney. *Kidney Int.* 17:756–763.
34. Hokin, M. R. 1967. The Na^+, K^+ and Cl^- content of goose salt gland slices and the effects of acetylcholine and ouabain. *J. Gen. Physiol.* 50:2197–2209.
35. Peaker, M. 1971. Intracellular concentrations of sodium, potassium and chloride in the salt-gland of the domestic goose and their relation to the secretory mechanism. *J. Physiol. (Lond.).* 213:399–410.
36. Rick, R., A. Dörge, A. D. C. MacKnight, A. Leaf, and K. Thurau. 1978. Electron microprobe analysis of the different epithelial cells of toad urinary bladder. *J. Membr. Biol.* 39:257–271.
37. Rick, R., A. Dörge, E. von Arnim, and K. Thurau. 1978. Electron microprobe analysis of frog skin epithelium: evidence for a syncytial sodium transport compartment. *J. Membr. Biol.* 29:313–331.
38. Zadunaisky, J. A., K. R. Spring, and T. Shindo. 1979. Intracellular chloride activity in the corneal epithelium. *Fed. Proc.* 38:1059. (Abstr.)
39. Frizzell, R. A., M. J. Welsh, and P. L. Smith. 1981. Electrophysiology of chloride-secreting epithelia. *In* Ion Transport by Epithelia. S. G. Schultz, editor. Raven Press, New York.

137–149.
40. Klyce, S. D., and R. K. S. Wong. 1977. Site and mode of adrenalin action on chloride transport across the rabbit corneal epithelium. *J. Physiol. (Lond.).* 266:777–799.
41. Nagel, W., and P. Reinach. 1980. Mechanism of stimulation by epinephrine of active transepithelial Cl transport in isolated frog cornea. *J. Membr. Biol.* 56:73–79.
42. Silva, P., J. Stoff, and F. H. Epstein. 1979. Indirect evidence for enhancement of Na-K-ATPase activity with stimulation of rectal gland secretion. *Am. J. Physiol.* 237:F468–F472.
43. Shorofsky, S., M. Field, and H. Fozzard. 1980. Electrophysiological studies of canine tracheal epithelium. *J. Gen. Physiol.* 76:27*a*. (Abstr.)
44. Ernst, S. A., C. C. Goertmiller, Jr., and R. A. Ellis. 1967. The effect of salt regimens on the development of (Na^+-K^+)-dependent ATPase activity during the growth of salt glands of ducklings. *Biochim. Biophys. Acta.* 135:682–692.
45. Rick, R., A. Dörge, F. Beck, and K. Thurau. 1982. Intracellular electrolyte concentration of frog cornea epithelium at different functional states of Cl-secretion. *Pflügers Arch. Eur. J. Physiol.* 392(Suppl.):R20.
46. Stewart, D. J., J. Sax, R. Funk, and A. K. Sen. 1979. Possible role of a cyclic GMP in stimulus-secretion coupling by salt gland of the duck. *Am. J. Physiol.* 237:C200–C204.
47. Civan, M. M. 1981. Intracellular potassium in toad urinary bladder: the recycling hypothesis. *In* Epithelial Ion and Water Transport. A. D. C. MacKnight and J. P. Leader, editors. Raven Press, New York. 107–116.